DOI: 10.1002/anie.201005458

Ferromagnetic Semiconductors

Structural-Distortion-Driven Cooperative Magnetic and Semiconductor-to-Insulator Transitions in Ferromagnetic $FeSb_2Se_4$**

Honore Djieutedjeu, Pierre F. P. Poudeu, Nathan J. Takas, Julien P. A. Makongo, Aurelian Rotaru, Kulugammana G. S. Ranmohotti, Clarence J. Anglin, Leonard Spinu, and John B. Wiley*

Transition metal compounds exhibiting spontaneous drops in magnetization are being investigated for use as molecular switches, sensors, and data storage devices. This phenomenon of magnetization change is generally associated with spin transition or spin crossover (high spin to low spin) induced by temperature, pressure, or irradiation, and is generally found in insulating antiferromagnetic oxides[1–5] and in transition metal complexes containing $3d^n$ ($4 \le n \le 7$) ions, such as iron(II), iron(III), or cobalt(III),[3,6–13] in octahedral or square-planar coordination.[2,4,11,14] Spontaneous loss of magnetization can also be induced by other mechanisms, such as the spin dimerization observed in $CuIr_2S_4$,[15] the so-called spin-Peierls transition[16–19] observed in $CuGeO_3$, and the Verwey transition,[20–22] which is commonly observed in mixed-valence transition metal oxides with the AB_2X_4 spinel or inverse spinel structures such as magnetite (Fe_3O_4).[23] The loss of magnetization in Verwey compounds is accompanied by a metal-to-insulator transition, which is interpreted as resulting from long-range ordering of the mixed-valence ions within the B sites of the spinel structure.[24]

Herein we present the observation of room-temperature ferromagnetism, semiconductivity, and reversible, cooperative magnetic and semiconductor-to-insulator (SI) transitions in $FeSb_2Se_4$. To the best of our knowledge, the coexistence of these phenomena in a single transition metal chalcogenide compound has not been reported to date. Despite the analogy of stoichiometry between $FeSb_2Se_4$ and $CuIr_2S_4$[15] and the similarity in the formal distribution of charges between $Fe^{2+}(Sb^{3+})_2(Se^{2-})_4$ and $Fe^{2+}(Fe^{3+})_2(O^{2-})_4$ (magnetite), the crystal structures of these compounds are profoundly different and none of the mechanisms mentioned above is suitable for the interpretation of the phase transitions observed in the three-dimensional monoclinic structure of $FeSb_2Se_4$. Therefore, alternative mechanisms to explain the observed transitions must be explored. Because the nature of the phase transitions in $FeSb_2Se_4$ can be rather complex, we have tackled the problem by performing systematic investigations of 1) the crystal structure above and below the transition temperature, 2) the thermal evolution of unit cell parameters using X-ray diffraction on powder and on single-crystal samples, 3) the electrical resistivity, and 4) the magnetic properties across the transition temperature.

$FeSb_2Se_4$ (see Supporting Information[25] for experimental details) crystallizes in the monoclinic space group *C*2*m* (No. 12) with lattice parameters $a = 13.069(3)$ Å, $b = 3.9671(8)$ Å, $c = 15.192(4)$ Å, and $\beta = 114.99(3)°$, and it is isostructural with $MnSb_2S_4$.[26] The structure contains four crystallographically independent metal positions and four Se positions. All metal sites located at special positions (Fe(3) at $(0,{}^1/_2,{}^1/_2)$ and Fe(4) at (0,0,0)) showed strong preference for the iron atom. The Fe(3) position is fully occupied by Fe, whereas the Fe(4) position contains some Sb in the ratio 85 % (Fe) to 15 % (Sb). Both Fe positions are coordinated by six selenium atoms with Fe(3) located in a distorted $[2+4]$ octahedral geometry with two short axial bonds and four long equatorial bonds, whilst Fe(4) is found in an almost regular octahedral geometry with interatomic distances ranging between 2.680(2) and 2.704(1) Å (Supporting Information, Table S1). In the structure, $\{M\}Se_6$ octahedra (M = Fe or Fe/Sb) share edges to form one-dimensional chains running along the *b* axis. $[\{Fe(4)\}Se_6]_\infty$ chains are interconnected by the Sb(2) atom in a distorted $[1+2+2+1]$ octahedral coordination of Se atoms to build a layer denoted A (Figure 1a). Likewise, $[\{Fe(3)\}Se_6]_\infty$ chains are linked by the Sb(1) atom in a distorted $[1+2+2]$ square pyramid of Se atoms to form layer B, which alternates with layer A along the *c* axis. Because of the partial Sb substitution at the Fe(4) position (0,0,0), the remaining Fe atoms (ca. 15 %) are distributed almost equally in both Sb positions with the ratio of 96 % (Sb) to 4 % (Fe) (Supporting Information, Table S2). The refined formula of the compound (Supporting Information, Table S3) and bond valence sum calculations[27] (Supporting Information, Table S4) indicate +2, +3, and −2 oxidation states for Fe, Sb, and Se, respectively.

As shown in Figure 2a, $FeSb_2Se_4$ remains ferromagnetic over the entire measured temperature range from 2 K to

[*] H. Djieutedjeu, Prof. P. F. P. Poudeu, Dr. N. J. Takas, Dr. J. P. A. Makongo, Dr. A. Rotaru, C. J. Anglin, Prof. L. Spinu, Prof. J. B. Wiley
The Advanced Materials Research Institute
University of New Orleans
2000 Lakeshore Dr., New Orleans, LA, 70148 (USA)
Fax: (+1) 5042803185
E-mail: ppoudeup@uno.edu
Homepage: http://fs.uno.edu/ppoudeup/
H. Djieutedjeu, Prof. P. F. P. Poudeu, Dr. K. G. S. Ranmohotti, C. J. Anglin, Prof. J. B. Wiley
Department of Chemistry, University of New Orleans
Dr. A. Rotaru, Prof. L. Spinu
Department of Physics, University of New Orleans

[**] This work was supported by the National Science Foundation (CAREER Award DMR-0954817).

Supporting information for this article is available on the WWW under http://dx.doi.org/10.1002/anie.201005458.

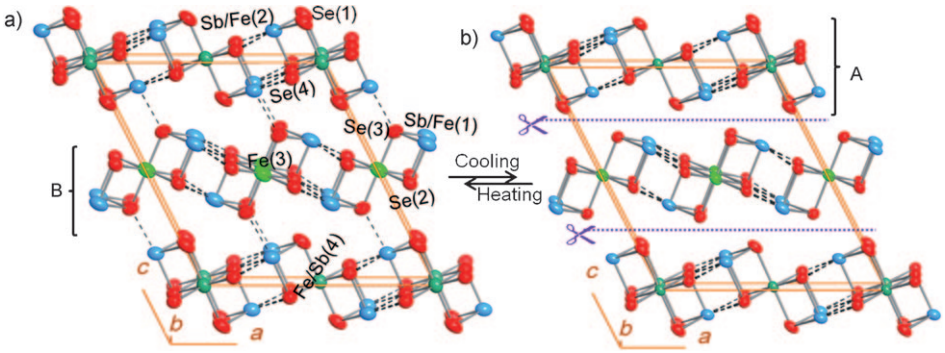

Figure 1. a, b) Representations of the crystal structures of $FeSb_2Se_4$ at 300 K (a) and 120 K (b); ellipsoids set at 98% probability for all atoms. To highlight the difference between the structures, a bond threshold of 3.12 Å was used. The structure reversibly distorts from a three-dimensional (3D) network to a two-dimensional (2D) layered structure upon cooling to 120 K due to the expansion (weakening) of the Sb(2)–Se(3) bond connecting adjacent layers A and B.

300 K. The susceptibility increases slowly with decreasing temperature down to about 130 K, at which point a spontaneous drop on the susceptibility is observed. From 130 K to about 10 K, the susceptibility remains almost constant, and slightly increases below 10 K (FC curve). Interestingly, AC magnetic susceptibility data revealed that the drop in the magnetization is recovered almost without hysteresis upon warming the sample through the transition temperature (Figure 2a, inset), indicating the reversible character of the magnetic transition at 130 K in $FeSb_2Se_4$. To further investigate the nature of the transition around 130 K, we have carried out isothermal magnetization at various temperatures between 2 K and 300 K (Figure 3a; Supporting Information, Figure S1). Magnetization data at 2 K shows a mild hysteresis with coercivity of about 700 Oe, which is typical for a soft ferromagnet. The magnetization curve at room temperature still showed a hysteresis with a sizable coercivity of about 300 Oe and a saturation magnetization value of about 500 emu mol^{-1} at an applied field of 15 kOe, thus confirming the ferromagnetic behavior of $FeSb_2Se_4$ at room temperature. The sizable values of the magnetic susceptibility (Figure 2a) and coercivity at 300 K suggest a fairly high ferromagnetic ordering temperature for $FeSb_2Se_4$. Careful examination of isothermal magnetization curves around the transition temperature (Supporting Information, Figure S1) revealed that the hysteresis shape is conserved above and below the transition. Furthermore, the coercivity of $FeSb_2Se_4$ slowly increases with decreasing temperature, drops spontaneously around 150 K, and increases rapidly thereafter with further cooling (Figure 3b). The above findings suggest that the ferromagnetism of the compound is maintained after the transition.

To understand the magnetic behavior of $FeSb_2Se_4$, we have examined the coupling between spins located on adjacent Fe atoms using the Goodenough–Kanamori rules.[28–30] As described above, the geometry of the Fe(3) and Fe(4) coordination polyhedron and also the length of Fe–Se bonds are very different. These parameters can influence the crystal field splitting energy (Δ_o) and thus the ordering of the iron $3d^6$ orbitals, as well as the spin distribution within the orbitals. Along this line, the [$FeSe_{2+4}$] geometry of the octahedral coordination around Fe(3) suggests a Jahn–Teller distortion of $3d^6$ orbitals with spin distribution of $(d_{xy})^2(d_{xz}, d_{yz})^1(d_{x^2-y^2})^1(d_{z^2})^1$, leading to a total spin value of $S=2$ (high spin), whilst the almost-perfect [$FeSe_6$] configuration of the octahedral coordination of Fe(4) suggests an octahedral splitting of $3d^6$ orbitals with a spin distribution of $(d_{xz}, d_{yz}, d_{xy})^2(d_{z^2}, d_{x^2-y^2})^0$ corre-

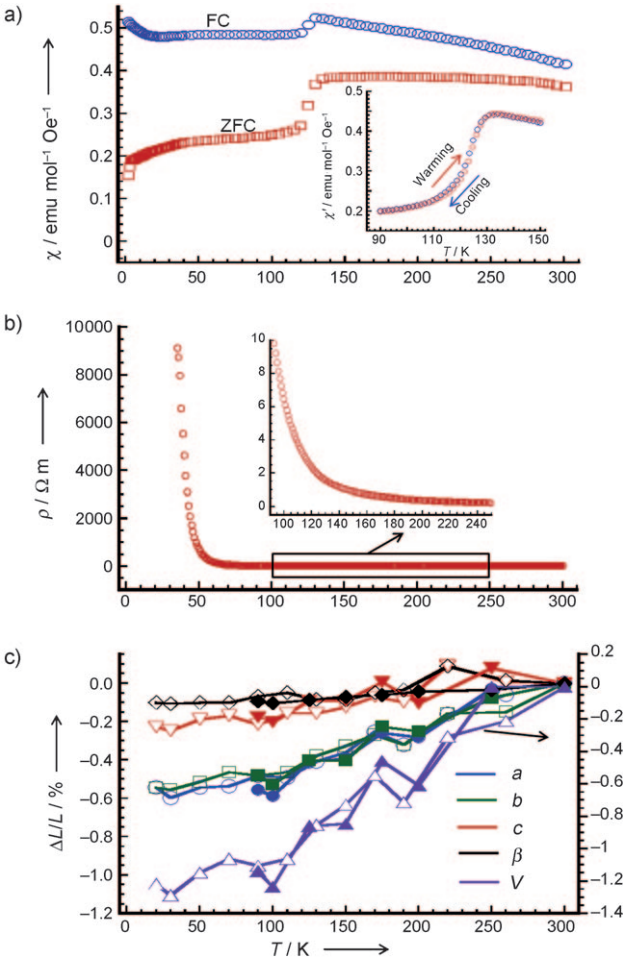

Figure 2. Manifestation of anisotropic lattice-distortion-driven magnetic and semiconductor–insulator transitions in $FeSb_2Se_4$. a) Field cooled (FC) and zero-field-cooled (ZFC) magnetic susceptibility, showing a magnetic transition at about 130 K. The observed drop in magnetization is reversible as indicated by the AC magnetic susceptibility on cooling and warming (see inset in (a)). b) Temperature-dependent electrical resistivity, showing spontaneous jumps at 130 K and 50 K. c) Thermal behavior of the unit cell parameters between 300 K and 20 K, showing preferential lattice contraction within the *ab* plane. $\Delta L/L$ represents the relative contraction of unit cell parameters *a*, *b*, *c*, and β as well as the unit cell volume *V* upon cooling. Open symbols: from X-ray powder patterns; filled symbols: from single-crystal X-ray analysis.

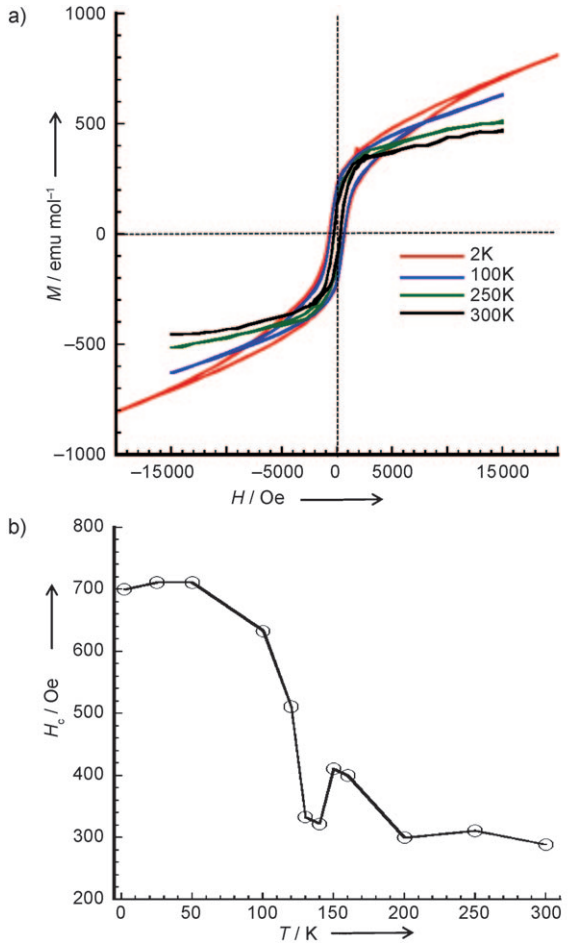

Figure 3. Ferromagnetic behavior of $FeSb_2Se_4$ between 2 K and 300 K. a) Field-dependent isothermal magnetization of $FeSb_2Se_4$ measured at 2 K, 100 K, 250 K, and 300 K with applied fields of up to 15 kOe. The ferromagnetic behavior of compound is maintained above and below the transition temperature (130 K). b) Temperature dependence of the coercivity of $FeSb_2Se_4$, showing a spontaneous drop at about 150 K.

sponding to a total spin value of $S=0$ (low spin). Therefore, the structure can be viewed as a bistable system consisting of diamagnetic layers A of Fe(4) atoms in a low-spin state ($S=0$) alternating along the *c* axis with the magnetic layers B of Fe(3) atoms in a high-spin state ($S=2$). Adjacent magnetic layers B are isolated magnetically from each other by the large distance of 15.192(3) Å between them. Therefore, the magnetic properties of $FeSb_2Se_4$ are controlled by exchange interactions between magnetic ions within layer B (intralayer interactions). However, $[\{Fe(3)\}Se_6]_\infty$ chains building layer *B* are about 6.829 (2) Å apart suggesting weak interchain interactions. The magnetic properties of $FeSb_2Se_4$ therefore depend on the nature and magnitude of intrachain exchange interactions between adjacent magnetic ions. Along the chain (*b* axis), the Fe(3)–Fe(3) distance of 3.967(2) Å is too long for direct magnetic exchange interactions between the magnetic moments on neighboring Fe atoms. Therefore, adjacent Fe(3) atoms are magnetically coupled via indirect exchange interactions through the bridging Se(2) atom. The observed Fe(3)-Se(2)-Fe(3) angle of 93.6 (1)° suggests weak ferromagnetic coupling of spins located on adjacent Fe atoms in an individual chain. This analysis is consistent with the small values of magnetic susceptibility and magnetization measured around 300 K.

The drop in magnetic susceptibility observed around 130 K in $FeSb_2Se_4$ is accompanied by a sharp increase of the electrical resistivity (semiconductor–insulator transition) at about the same temperature. As shown in Figure 2b and Supporting Information, Figure S2, $FeSb_2Se_4$ at room temperature is a narrow band gap semiconductor with electrical resistivity of 0.16 Ω m and an optical band gap of 0.33 eV. The electrical resistivity initially increases slowly with decreasing temperature down to about 130 K, after which a rapid increase by an order of magnitude is observed. As the temperature decreases further, a sharper jump by four orders of magnitude in the resistivity occurs around 50 K and an out-of-range resistivity (>10 kΩ m) is reached below 35 K (Figure 2b). The sharp increase in the electrical resistivity of $FeSb_2Se_4$ suggests a semiconductor-to-insulator (SI) transition. The observed simultaneous change in the magnetic susceptibility and electrical resistivity around 130 K suggests that both transition processes in $FeSb_2Se_4$ are induced by the same driving force.

To understand the nature and the origin of the transitions in the magnetic susceptibility and electrical resistivity data and to examine the possibility of a structural phase change that may be responsible for these transitions, we carried out X-ray diffraction experiments on powder (XRPD) and on a single crystal at temperatures between 20 K and 300 K and have determined the thermal evolution of the lattice parameters. Furthermore, we have also performed the structure determination of $FeSb_2Se_4$ at 120 K (below the transition at 130 K). The powder diffraction patterns were recorded on heating and on cooling and all peaks were indexed with the monoclinic structure of $FeSb_2Se_4$. No appearance/disappearance of small peaks or peak splitting that would suggest breaking of symmetry could be detected above the XRD background (Supporting Information, Figure S3). The refinement of the unit cell parameters at various temperatures reveals fast contraction of the *a* and *b* parameters upon cooling (Figure 2c), whilst the *c* parameter and β angle first expand and then contract slowly with decreasing temperature. This effect suggests an increase in the strength of anisotropic distortion of the unit cell parameters with decreasing temperature. Similar thermal evolution of the unit cell parameters was also observed on single-crystal data (Figure 2c). The observed anisotropic lattice distortion in $FeSb_2Se_4$ is reversible without hysteresis upon heating (Supporting Information, Tables S5 and S6). The absence of symmetry breaking upon cooling suggests that the transition observed around 130 K in the magnetic and resistivity data of $FeSb_2Se_4$ does not induce major structural changes.

The structure of $FeSb_2Se_4$ at 120 K was determined using the same single crystal employed for the structure determination at 300 K. Analysis of diffraction data indicated no change in the crystal symmetry (monoclinic space group *C*2*m*), and the contraction of unit cell parameters is consistent with XRPD results (Supporting Information, Table S3). The structure at 120 K was refined using structural parameters of

$FeSb_2Se_4$ obtained at 300 K as the starting model. The overall quality of the fit was excellent (Supporting Information, Table S3), and indicates that no major structural changes occur upon cooling through the transition temperature. The refined structure of $FeSb_2Se_4$ at 120 K and 300 K drawn using a M–Se (M = Fe, Sb) bond threshold of 3.12 Å (longest Sb–Se bond at 300 K) are compared in Figure 1. To detect structural differences that might provide some insights on the origin and the underlying mechanism of the observed magnetic and SI transitions, we have carefully analyzed the variation of chemical bonding within the structure of $FeSb_2Se_4$ upon cooling below the transition temperature at 130 K (Supporting Information, Table S1). The direct consequence of the strong preferential contraction of the *a* and *b* parameters upon cooling through the transition temperature is the sharp decrease in the length of all interatomic bonds parallel to the *ab* plane, whilst interatomic bonds parallel to the *c* axis only showed marginal contraction. The strong preferential contraction within the *ab* plane induces an anomalous expansion of the equatorial Sb(2)–Se(3) bond bridging layers A and B, from 3.118(2) Å at 300 K to 3.123(1) Å at 120 K.

In heavy main group metal chalcogenides with a high degree of covalency, such as the $FeSb_2Se_4$ phase, the balance of short- and long-range interactions is strongly related to the electronic subsystem. Therefore, a small change in the lattice parameters could disturb the electronic subsystem, inducing the spontaneous changes in the electrical resistivity observed in $FeSb_2Se_4$. For instance, careful examination of the structures of $FeSb_2Se_4$ above and below the transition temperature of 130 K showed that the preferential contraction within the *ab* plane causes the weakening (electronically) of the connectivity between layers A and B (Sb(2)–Se(3)) leading to a distortion of the structure from the three-dimensional (3D) network (Figure 1a) to a two-dimensional (2D) layered structure (Figure 1b). This reduction of dimensionality from 3D to 2D is believed to be responsible for the fast increase in the electrical resistivity observed around 130 K (Figure 2b). The weakening of the Sb(2)–Se(3) bond presumably increases the band gap of the material, which translates into an increase in the electrical resistivity. As the structure continues to distort upon cooling (increasing the $\Delta c/c$ to $\Delta a/a$ ratio; Figure 2c), we anticipate further increases in the length of the Sb(2)–Se(3) bond, leading to a larger gap between layers A and B. This mechanism is consistent with the sharp increase in electrical resistivity observed below 50 K.

As discussed above, the magnetic behavior of $FeSb_2Se_4$ is controlled by indirect exchange interactions between adjacent Fe(3) atoms within individual chains building layer B. The nature and magnitude of the indirect magnetic exchange interactions strongly depend on the Fe(3)-Se(2)-Fe(3) angle.[28–30] In $FeSb_2Se_4$, the observed preferential contraction within the *ab* plane causes the Fe(3)-Se(2)-Fe(3) angle to increase slightly (from 93.6(1) at 300 K to 93.8(1) at 120 K). This increase of angle favors antiferromagnetic coupling of spins located on adjacent Fe atoms in an individual chain at the expense of weak ferromagnetic interactions, resulting in the observed drop in the magnitude of the magnetic susceptibility below 130 K.

The driving force behind the anisotropic lattice contraction (Figure 2c) in $FeSb_2Se_4$ upon cooling, which leads to the observed complex and reversible ordering pattern is yet to be understood. However, by looking carefully at the geometry of the $\{Sb(2)\}Se_6$ octahedron bridging layers A and B, we can see that the Sb(2)–Se(3) bond expands (rather than contracting) on cooling below the transition at 130 K. Therefore, we can speculate that the stereoactivity of the Sb $5s^2$ lone pair, which is manifested by the expansion of the Sb(2)–Se(3) axial bond (parallel to the *c* axis) is a possible "force" resisting the fast contraction of the *c* parameter and β angle upon cooling. Presumably the volume of the $\{Sb(2)\}Se_6$ octahedron near 300 K is the critical size for the stability of Sb $5s^2$ lone pair and further contraction upon cooling is opposed by an increased stereoactivity of the lone pair. This mechanism is consistent with the observed increase in the degree of lattice distortion in $FeSb_2Se_4$ at temperatures below the transition.

In summary, we have found that the most interesting feature of the $FeSb_2Se_4$ phase is the coexistence of room-temperature ferromagnetism and semiconductivity, with a remarkable interplay between reversible magnetic ordering phenomena and semiconductor-to-insulator (SI) transition upon cooling. The observed cooperative magnetic and SI transitions in $FeSb_2Se_4$ are driven by local isostructural distortions arising from the preferential lattice contraction within the *ab* plane. Such a cooperative transition, to our knowledge, has no precedent in pure inorganic materials and represents a significant increase in the level of complexity with respect to known phase transitions. The sizable difference between the magnetic susceptibility and electrical resistivity of $FeSb_2Se_4$ above and below the transition of 130 K shows great promise for application as highly sensitive temperature sensors through the detection of change in the intensity of magnetic and/or electrical responses. Furthermore, the high chemical and thermal stability of $FeSb_2Se_4$ (Supporting Information, Figure S4) are favorable for processing into molecular-based devices. It is also interesting to note the stability of the monoclinic structure throughout the anisotropic contraction, which points to the exciting prospect of inducing similar magnetic and SI transitions around room temperature by stretching the material along the *c* axis or through application of weak pressure perpendicular to *ac* and/or *bc* planes. It would be interesting to investigate these points experimentally. Another important feature of the $FeSb_2Se_4$ phase is the bistability of Fe atoms in the structure where layers of Fe(3) atoms (layer B) in high-spin state ($S = 2$) and Fe(4) atoms (layer A) in low-spin state ($S = 0$) alternate along the *c* axis. This unique feature could provide a new degree of flexibility and control to the design of next generation molecular memory[8,31–34] and data storage devices.[34]

Received: August 31, 2010
Published online: November 24, 2010

Keywords: chalcogenides · ferromagnetism · magnetic transitions · semiconductors · transition metals

[1] T. Kawakami, Y. Tsujimoto, H. Kageyama, X. Q. Chen, C. L. Fu, C. Tassel, A. Kitada, S. Suto, K. Hirama, Y. Sekiya, Y. Makino, T. Okada, T. Yagi, N. Hayashi, K. Yoshimura, S. Nasu, R. Podloucky, M. Takano, *Nat. Chem.* **2009**, *1*, 371.

[2] J. Badro, G. Fiquet, F. Guyot, J. P. Rueff, V. V. Struzhkin, G. Vanko, G. Monaco, *Science* **2003**, *300*, 789.

[3] P. Gütlich, H. A. Goodwin, *Top. Curr. Chem.* **2004**, *232–242*, 233.

[4] J. F. Lin, V. V. Struzhkin, S. D. Jacobsen, M. Y. Hu, P. Chow, J. Kung, H. Z. Liu, H. K. Mao, R. J. Hemley, *Nature* **2005**, *436*, 377.

[5] J. Li, V. V. Struzhkin, H. Mao, J. Shu, R. J. Hemley, Y. Fei, B. Mysen, P. Dera, V. Prakapenka, G. Shen, *Proc. Natl. Acad. Sci. USA* **2004**, *101*, 14027.

[6] P. Gütlich, Y. Garcia, H. A. Goodwin, *Chem. Soc. Rev.* **2000**, *29*, 419.

[7] E. König in *Progress in Inorganic Chemistry*, *Vol. 35* (Ed.: S. J. Lippard), John Wiley and Sons, New York, **1987**, p. 527.

[8] O. Kahn, J. Krober, C. Jay, *Adv. Mater.* **1992**, *4*, 718.

[9] P. Gütlich, A. Hauser, H. Spiering, *Angew. Chem.* **1994**, *106*, 2109; *Angew. Chem. Int. Ed. Engl.* **1994**, *33*, 2024.

[10] J. A. Real, A. B. Gasper, V. Niel, M. C. Munoz, *Coord. Chem. Rev.* **2003**, *236*, 121.

[11] J. A. Real, E. Andres, M. C. Munoz, M. Julve, T. Granier, A. Bousseksou, F. Varret, *Science* **1995**, *268*, 265.

[12] J. F. Létard, P. Guionneau, E. Codjovi, O. Lavastre, G. Bravic, D. Chasseau, O. Kahn, *J. Am. Chem. Soc.* **1997**, *119*, 10861.

[13] K. Boukheddaden, I. Shteto, B. Hoo, F. Varret, *Phys. Rev. B* **2000**, *62*, 14796.

[14] G. J. Halder, C. J. Kepert, B. Moubaraki, K. S. Murray, J. D. Cashion, *Science* **2002**, *298*, 1762.

[15] P. G. Radaelli, Y. Horibe, M. J. Gutmann, H. Ishibashi, C. H. Chen, R. M. Ibberson, Y. Koyama, Y. S. Hor, V. Kiryukhin, S. W. Cheong, *Nature* **2002**, *416*, 155.

[16] J. W. Bray, H. R. Hart, L. V. Interrante, I. S. Jacobs, J. S. Kasper, G. D. Watkins, S. H. Wee, J. C. Bonner, *Phys. Rev. Lett.* **1975**, *35*, 744.

[17] I. S. Jacobs, J. W. Bray, H. R. Hart, L. V. Interrante, J. S. Kasper, G. D. Watkins, D. E. Prober, J. C. Bonner, *Phys. Rev. B* **1976**, *14*, 3036.

[18] M. Hase, I. Terasaki, K. Uchinokura, *Phys. Rev. Lett.* **1993**, *70*, 3651.

[19] K. Hirota, D. E. Cox, J. E. Lorenzo, G. Shirane, J. M. Tranquada, M. Hase, K. Uchinokura, H. Kojima, Y. Shibuya, I. Tanaka, *Phys. Rev. Lett.* **1994**, *73*, 736.

[20] J. García, G. Subias, *J. Phys. Condens. Matter* **2004**, *16*, R145.

[21] F. Walz, *J. Phys. Condens. Matter* **2002**, *14*, R285.

[22] J. E. W. Verwey, *Nature* **1939**, *144*, 327.

[23] W. H. Bragg, *Nature* **1915**, *95*, 561.

[24] M. Imada, A. Fujimori, Y. Tokura, *Rev. Mod. Phys.* **1998**, *70*, 1039.

[25] The Supporting Information contains Materials and Experimental Methods, Tables S1–S6, and Figures S1–S4.

[26] A. Pfitzner, D. Kurowski, *Z. Kristallogr.* **2000**, *215*, 373.

[27] N. E. Brese, M. O'Keeffe, *Acta Crystallogr. Sect. B* **1991**, *47*, 192.

[28] J. B. Goodenough, *J. Phys. Chem. Solids* **1958**, *6*, 287.

[29] J. B. Goodenough, *Phys. Rev.* **1955**, *100*, 564.

[30] J. Kanamori, *J. Phys. Chem. Solids* **1959**, *10*, 87.

[31] P. Gütlich, A. Hauser, *Coord. Chem. Rev.* **1990**, *97*, 1.

[32] O. Kahn, C. J. Martinez, *Science* **1998**, *279*, 44.

[33] E. König, G. Ritter, S. K. Kulshreshtha, *Chem. Rev.* **1985**, *85*, 219.

[34] J. F. Letard, P. Guionneau, L. Goux-Capes in *Spin Crossover in Transition Metal Compounds III*, *Vol. 235*, Springer, Berlin, **2004**, p. 221.

